Electrolytes for Solid-Oxide Fuel Cells

Harumi Yokokawa, Natsuko Sakai, Teruhisa Horita, Katsuhiko Yamaji, and M.E. Brito

Abstract

Three solid-oxide fuel cell (SOFC) electrolytes, yttria-stabilized zirconia (YSZ), rare-earth–doped ceria (REDC), and lanthanum strontium gallium magnesium oxide (LSGM), are reviewed on their electrical properties, materials compatibility, and mass transport properties in relation to their use in SOFCs. For the fluorite-type oxides (zirconia and ceria), electrical properties and thermodynamic stability are discussed in relation to their valence stability and the size of the host and dopant ions. Materials compatibility with electrodes is examined in terms of physicochemical features and their relationship to the electrochemical reactions. The application of secondary ion mass spectrometry (SIMS) to detect interface reactivity is demonstrated. The usefulness of doped ceria is discussed as an interlayer to prevent chemical reactions at the electrode–electrolyte interfaces and also as an oxide component in Ni–cermet anodes to avoid carbon deposition on nickel surfaces. Finally, the importance of cation diffusivity in LSGM is discussed, with an emphasis on the grain-boundary effects.

Keywords: *conductivity, diffusion, electrolytes, materials compatibility, solid-oxide fuel cells.*

Introduction

The most important breakthrough in solid-oxide fuel cells (SOFCs) was made by researchers at the Westinghouse Electric Company in the mid-1980s.[1] Optimization of materials led to yttria-stabilized zirconia (YSZ) as the favored electrolyte. The most important property of a SOFC electrolyte is its oxide ionic conductivity. Although rare-earth–doped ceria (REDC) exhibits higher oxide ion conductivity than YSZ, doped ceria is less stable. In 1994, a new electrolyte, $LaGaO_3$-based perovskite, was invented. Extensive investigation revealed that proper functioning of this electrolyte depends upon its interaction with other components in the fuel cell.

Only a few materials have survived as practical SOFC electrolytes because many electrical, electrochemical, mechanical, and chemical properties are required of a successful electrolyte. In this overview, we make an attempt to clarify how those different properties are closely related to each other. Particular emphases will be placed on materials compatibility and mass transport properties. These are crucial points in establishing the technologies associated with high-temperature fuel cells.[1]

Electrical Conductivities as a Key Property

For use as an electrolyte, the oxide ion conductivity, $\sigma(O^{2-})$, should be high and the electronic conductivity, σ_{el}, should be low.[2] Figure 1 shows $\sigma(O^{2-})$ and σ_{el} for yttria-stabilized zirconia (YSZ), Gd-doped ceria (GDC), and lanthanum strontium gallium magnesium oxide (LSGM) electrolytes at 1073 K. Oxide ion conductivity $\sigma(O^{2-})$ is independent of the oxygen potential. The electronic conductivity has two components: electron conductivity with –1/4 dependence (negative slope portion of the σ_{el} plot) and hole conductivity with +1/4 dependence (positive slope portion) in Figure 1. The most important feature of SOFC electrolytes is the conversion efficiency, $\varepsilon_{electrolyte}$, from chemical energy to electrical energy,[3,4] which is derived from the electrical properties of electrolyte as follows:

$$\varepsilon_{electrolyte} = \frac{J^{ext}V^{term}}{J_{O^{2-}}V^{TH}}, \quad (1)$$

where V^{term} and V^{TH} are the terminal voltage and the thermodynamically derived voltage, respectively, and J^{ext} and $J_{O^{2-}}$ are the external current and the oxide ion flux through the electrolyte, respectively. Here, electrode effects such as the electrode internal resistivity and the electrode reaction resistivity are not included. A low value of $\sigma(O^{2-})$ lowers V^{term} (corresponding to the Joule loss); a high value of σ_{el} lowers the $J^{ext}/J(O^{2-})$ ratio and also the V^{term} (this is called the loss due to electronic shorting or oxygen permeation). Both terms lead to lowering of $\varepsilon_{electrolyte}$. Among three materials, YSZ $[(ZrO_2)_{0.92}(Y_2O_3)_{0.08}]$ exhibits the lowest $\sigma(O^{2-})$; however, the extremely low σ_{el} causes only a small loss due to electronic shorting. To reduce the Joule loss due to the low $\sigma(O^{2-})$ values, a thinner electrolyte or higher operation temperature is favored. However, the shorting effect becomes significant when a thinner electrolyte is used and also increases with operational temperature because the activation energy for σ_{el} is usually higher than that for $\sigma(O^{2-})$. Figure 2 shows $\varepsilon_{electrolyte}$ as a function of temperature with a parameter of electrolyte thickness. The $\varepsilon_{electrolyte}$ is high enough only in a narrow temperature window. The lower-temperature side is limited by the low $\sigma(O^{2-})$, while the high-temperature side is limited by increasing σ_{el}.[5] For a 50-μm-thick YSZ film, a typical operation temperature of 1273 K is very close to a maximum

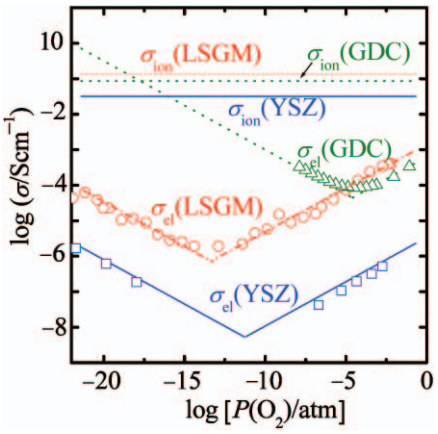

Figure 1. Oxide ion conductivity [$\sigma_{ion} = \sigma(O^{2-})$] and electronic (electron and hole) conductivities (σ_{el}) for YSZ [$(ZrO_2)_{0.92}(Y_2O_3)_{0.08}$] (blue curves, blue squares), GDC ($Ce_{0.8}Gd_{0.2}O_{1.9}$) (green curves, green triangles), and LSGM ($La_{0.8}Sr_{02}Ga_{0.8}Mg_{0.2}O_{2.8}$) (red curves, red circles) at 1073 K.

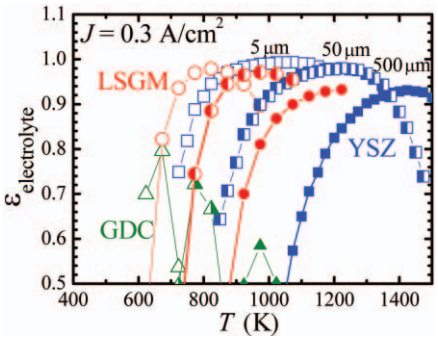

Figure 2. Conversion efficiency, $\varepsilon_{electrolyte}$, characterized in terms of the conductive properties of three solid-oxide fuel cell electrolytes at a given current density as a function of temperature, with electrolyte thicknesses of 5 μm (open symbols), 50 μm (half-solid symbols), and 500 μm (solid symbols) for YSZ [$(ZrO_2)_{0.92}(Y_2O_3)_{0.08}$] (blue squares), GDC ($Ce_{0.8}Gd_{0.2}O_{1.9}$) (green triangles), and LSGM ($La_{0.8}Sr_{02}Ga_{0.8}Mg_{0.2}O_{2.8}$) (red circles).

value for $\varepsilon_{electrolyte}$ within the narrow window (from 900 K to 1450 K).

GDC ($Ce_{0.8}Gd_{0.2}O_{1.9}$), in the same fluorite-type structure as YSZ, exhibits a higher $\sigma(O^{2-})$ than YSZ. Even so, σ_{el} in GDC[6] is about seven orders of magnitude higher than YSZ. This large σ_{el} makes GDC less appropriate than YSZ or LSGM as a SOFC electrolyte, as is clearly shown in Figure 2.

LSGM ($La_{0.8}Sr_{0.2}Ga_{0.8}Mg_{0.2}O_{2.8}$) was found in 1994 by Ishihara et al.[7] as a new electrolyte exhibiting a higher $\sigma(O^{2-})$ than YSZ; its σ_{el} is 2–3 orders of magnitude higher than YSZ,[8,9] but still low enough compared with its oxide ionic conductivity to make it a good SOFC electrolyte. Note that the hole conductivity in the oxidative atmosphere is the highest in LSGM among the three electrolytes; therefore, some decrease in $\varepsilon_{electrolyte}$ is expected in a high-pressure operation.

Valence Stability and the Effect of Ionic Size

Thermodynamic stability in the valence states and phases is also required for SOFC electrolytes. A good example is the valence stability of the trivalent ions of zirconium and cerium.[10] Ce^{3+} ions are relatively stable in the fluorite structure, compared with Zr^{3+}. This leads to the high electron conductivity of REDC in a reducing atmosphere, where Ce^{3+} ions become relatively stable. Ce^{3+} ions also cause volume expansion, leading to severe mechanical instability.

For tetravalent ions, an interesting difference originating from the ionic size appears between Zr^{4+} and Ce^{4+}. Zr^{4+} ions are somewhat small to occupy those cation sites in the fluorite lattice that have eight oxide ions as coordinates. As a result, the monoclinic phase having six oxide ion coordinates becomes more stable than the fluorite phase. When rare-earth oxides are doped to ZrO_2, the oxide ion vacancy is located preferably around Zr^{4+} ions rather than around the dopant rare-earth ions.[11] This is the origin of the thermodynamically large stabilization of rare-earth–doped zirconia.[10] In other words, rare-earth doping is effective in realizing the 6–7 oxide ion coordination around Zr^{4+} ions. On the other hand, Ce^{4+} ions are large enough to form the fluorite lattice so that the oxide ion vacancy tends to locate around the dopants.[12] This difference provides a good explanation for the dopant-dependence of $\sigma(O^{2-})$ and related properties and for the differences between the zirconia and ceria systems.[11–15]

Materials Compatibility

The electrolyte materials have interfaces with the cathode, anode, interconnect, and (if any) sealing materials. The chemical compatibility[16] of the electrolyte with these materials is the most important requirement for high-temperature fuel cells.[1] For example, preventing reactions of zirconia with the perovskite oxide cathode are crucial;[1,4,10,16] in an early stage of the research effort, $LaCoO_3$, which was known as an active electrode material, was found to react with ZrO_2 to form less-conductive $La_2Zr_2O_7$ and CoO. In Figure 3a, the generalized chemical potential diagram[17] in the La-Mn-Zr-O system at 1273 K is given as an example for investigating the thermodynamic stability of the interface between ZrO_2 and $LaMnO_3$;[18] the corresponding compositional phase diagram is also given and compared in Figure 3b. $LaMnO_3$ is unique in the sense that the oxidation of Mn^{3+} to Mn^{4+} can take place in the perovskite lattice, forming the vacancies in the La sites. This nonstoichiometry, $1 - y$, in $La_{1-y}MnO_3$ (A-site deficiency, y) is important, since good compatibility with ZrO_2 is obtained only at a large A-site deficiency. In the region that is less A-site–deficient, $La_2Zr_2O_7$ can be formed at the $ZrO_2/LaMnO_3$ interfaces. Such a reaction product at the interface can be detected by secondary ion mass spectrometry (SIMS), as shown in Figure 4. An oxygen isotope exchange experiment was made on a thin layer of $La_{0.9}Sr_{0.1}MnO_3$ (LSM) deposited on a single crystal of YSZ at a given temperature, and a quenched sample was sputtered by the primary ions. Then the respective secondary ions from the sample were detected as a function of sputtering time. The sputtering time can be correlated to the depth inside the sample, x, and the change in the intensity corresponds to change in concentration C across the interface. Figure 4 shows that a thin layer of $La_2Zr_2O_7$ was detected at the interface between YSZ and LSM.[19] The $La_2Zr_2O_7$ formation should be accompanied by the oxidation of the manganese ions in the perovskite lattice and the change in the La stoichiometry. This oxidative nature is important because in the cathode reaction, oxygen is reduced, leading to an oxygen potential shift at the cathode/electrolyte interface to the reducing side during fuel cell operation. Because of this shift, the oxidative reaction will lose its driving force, and as a result, $La_2Zr_2O_7$ formed at the interface will disappear from the interfaces. This behavior has been well confirmed by transmission electron microscopy.[20,21] In Figure 4, the intensity ratio R of $^{18}O/^{16}O$ rapidly decreases to

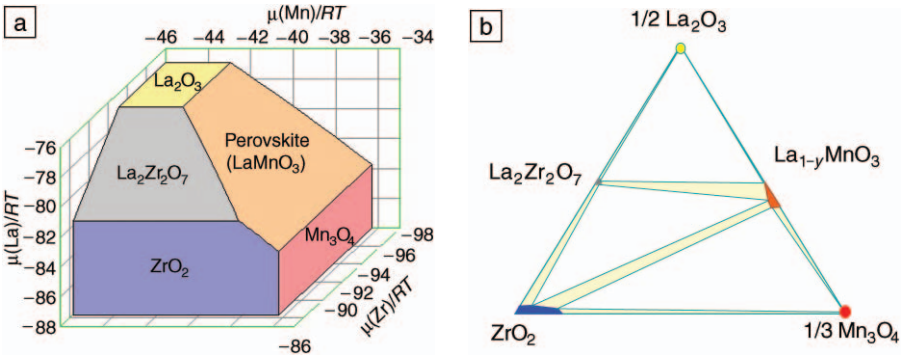

Figure 3. (a) Generalized chemical potential diagram[17] for the La-Mn-Zr-O system at $p(O_2) = 1$ atm, where the stability polygons for La_2O_3, ZrO_2, $LaMnO_3$, and $La_2Zr_2O_7$ are plotted using the elemental chemical potential axes, $\mu(M)/RT$, (M = Zr,La,Mn), R and T being the gas constant and temperature, respectively. (b) Corresponding compositional phase diagram.

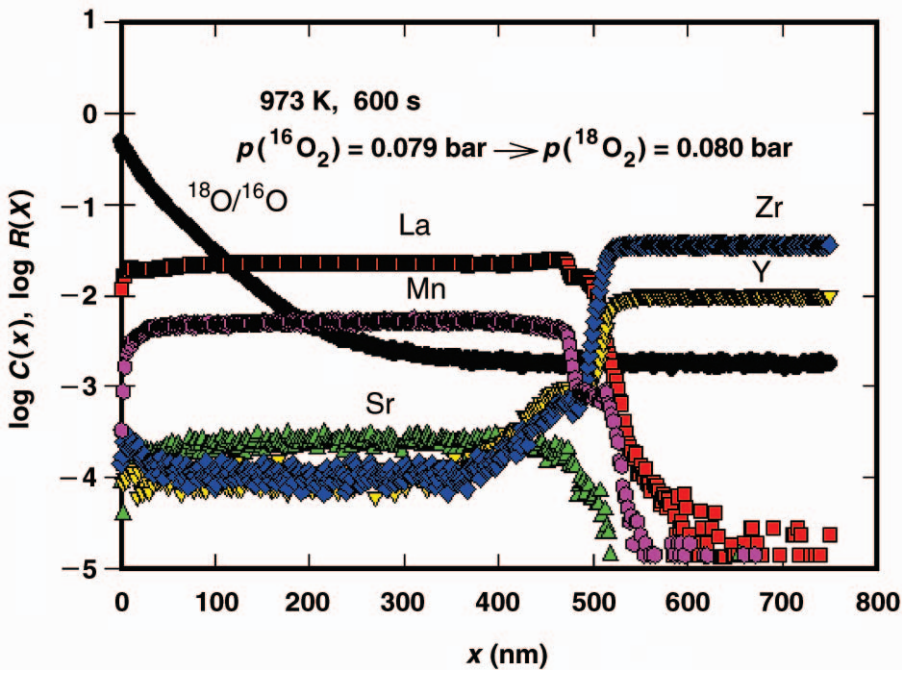

Figure 4. Secondary ion mass spectrometry analysis on oxygen diffusion at 973 K for dense $La_{0.9}Sr_{0.1}MnO_3$–YSZ system; at interfaces, a thin layer of $La_2Zr_2O_7$ was formed. C(x) *is the relative intensity of respective ions,* R(x) *is the intensity ratio of ^{18}O to ^{16}O;* x *is the depth from the surface of the $La_{0.9}Sr_{0.1}MnO_3$.*

the background level inside the LSM electrode, indicating that the oxide ion diffusion in the LSM electrode is not fast. As a result, the main cathode reaction proceeds at the cathode–electrolyte–gas three-phase boundary. In fact, SIMS analyses provide visualized oxygen flow in the three phase boundaries.[22]

Ceria as a Diffusion Barrier

Doped ceria is less reactive with the perovskite oxides than zirconia, because Ce^{4+} ions are too large to form double oxides with rare-earth oxides. Doped ceria can thus be used as an interlayer between YSZ and more active cathodes such as lanthanum strontium cobaltite (LSC) or lanthanum strontium cobaltite ferrite (LSCF). On the other hand, rare-earth dopants are not highly stabilized in the CeO_2 lattice.[15] As a result, the yttria component in doped ceria becomes more reactive than YSZ, and easily reacts, for example, with alumina to form yttrium aluminates. Furthermore, cation diffusion through doped ceria becomes important, because sintering of doped ceria is significantly enhanced in the presence of a small amount of transition-metal oxides such as Fe_2O_3[23] or CoO[24] and also because there exists a large driving force for La, Ca, and Sr to diffuse and form zirconates at ceria/zirconia interfaces.

Electrolyte–Electrode Interactions

Another interesting feature related to the electrolyte is the proton solubility in the fluorite-type oxides and its relation to electrochemical reactions. In polycrystalline samples, a two order-of-magnitude difference is observed in proton solubility between YSZ and yttria-doped ceria (YDC).[25] Interestingly, this magnitude difference is the same as those in the hole conductivity and the thermodynamic activity of $YO_{1.5}$.[15] This suggests that the dopant–oxide ion vacancy configuration, represented energetically by the thermodynamic activity of $YO_{1.5}$, $a(YO_{1.5})$, governs the formation of holes and protons as described in the following chemical reactions:[15]

Hole formation:

$$V_O^{\cdot\cdot} + 1/2\ O_2(g) = O + 2h^{\cdot} \quad (1)$$

$$2YO_{1.5}(\text{in fluorite}) + 1/2\ O_2(g) = 2YOO(\text{in fluorite}) \quad (2)$$

Proton formation:

$$V_O^{\cdot\cdot} + H_2O(g) = O + 2H^{\cdot} \quad (3)$$

$$2YO_{1.5}(\text{in fluorite}) + H_2O(g) = 2YOOH \quad (4)$$

Here, $V_O^{\cdot\cdot}$ is a vacancy on an oxygen site, $h^{\cdot}$ is a hole, and $H^{\cdot}$ is a proton. In the cathode reaction mechanism, it is not easy to determine the effects of protons or water vapor except in a few cases;[15] the chromium poisoning[26] on an LSM cathode appears in different ways between YSZ and GDC,[27] probably because protons in GDC slightly change the mass transfer and associated oxygen potential distribution around the three phase boundaries where chromium vapors attack.

In the anode reaction mechanism, the use of doped ceria is of technological interest for hydrocarbon fuels, because carbon deposition is usually prevented to a significant level in nickel ceria cermet electrodes. Again, the SIMS technique provides a powerful tool to detect the elemental distribution on a Ni electrode on YSZ and a Ni electrode on YDC in a gas mixture of CH_4, D_2O, and $^{18}O_2$.[28] The line profiles of respective ions from the Ni plate to the oxide surface are plotted as a function of location, x, in Figure 5. In Ni on YSZ, the hydrogen concentration is high in the nickel, and carbon is distributed on the nickel surface. This suggests that dissociation of CH_4 takes place on nickel and deposited carbon remains on the Ni surface, whereas the dissociated hydrogen dissolves into Ni. On the contrary, in Ni on YDC, the hydrogen concentration is low, approximately at the same level as that in the YDC. Furthermore, less carbon is deposited on the Ni surface compared with the Ni/YSZ case. These features can be interpreted as follows: Even when methane dissociation takes place on a Ni surface, hydrogen dissolved in Ni is further transferred into YDC; the resulting decrease in hydrogen concentration in the Ni may promote further dissociation, particularly dissociation of H_2O to form oxygen atoms on Ni. These oxygen atoms may then react with dissolved carbon atoms. As a result, the reforming reaction takes place on the Ni surface. This mechanism can explain why the presence of ceria tends to prevent carbon deposition on nickel surfaces.

Cation Diffusion in Lanthanum Gallate Electrolytes

The cation interdiffusion between $(La,Sr)(Ga,Mg)O_3$, LSGM, and the cathodes $(La,Sr)MnO_3$ or $(La,Sr)CoO_3$) is quite fast,[29] and NiO in the anode is dissolved into LSGM during the fabrication process.[30] A higher creep rate[31] in LSGM than in YSZ also indicates fast cation diffusivity. In contrast, recent experimental data on self-diffusion,[32] shown in Figure 6, has revealed that self-diffusivity in LSGM is in the same magnitude among the major components and is in good agreement

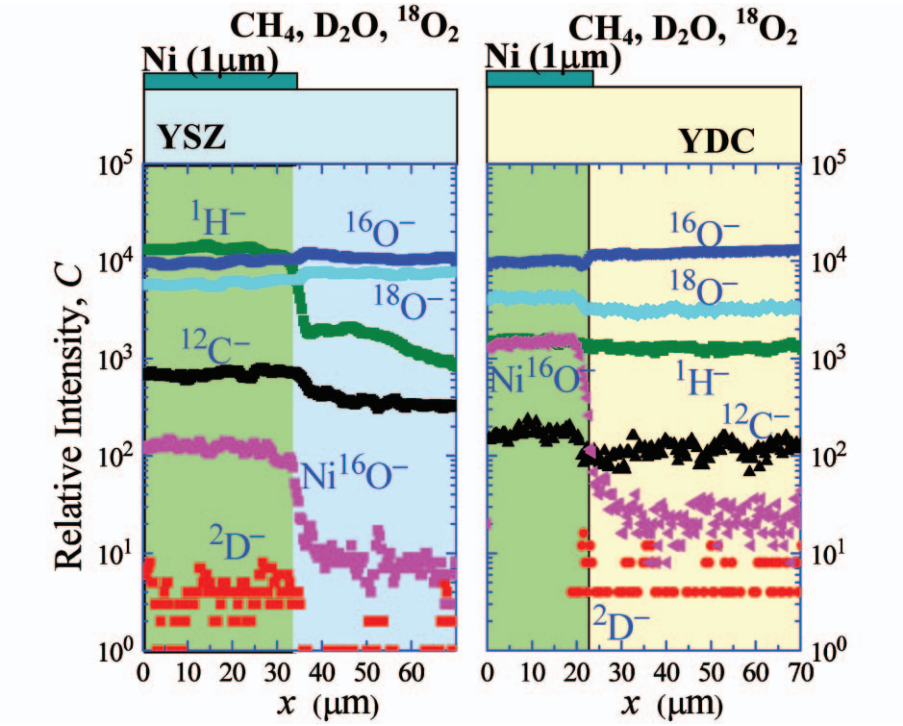

Figure 5. Elemental distributions given as SIMS counts (relative intensity) on Ni (1 μm thick)/YSZ and Ni/YDC(yttria-doped ceria) cermets detected by SIMS analysis after reactions with a gas mixture of CH_4, $^{18}O_2$, $D_2{}^{16}O$, and Ar at 973 K. The nickel oxide border can be judged from the line for $Ni^{16}O^-$ that exhibits a drastic decrease. The line profiles are plotted as a function of location (x) for $^{16}O^-$, $^{18}O^-$, $^1H^-$, $^2D^-$, and $^{12}C^-$.

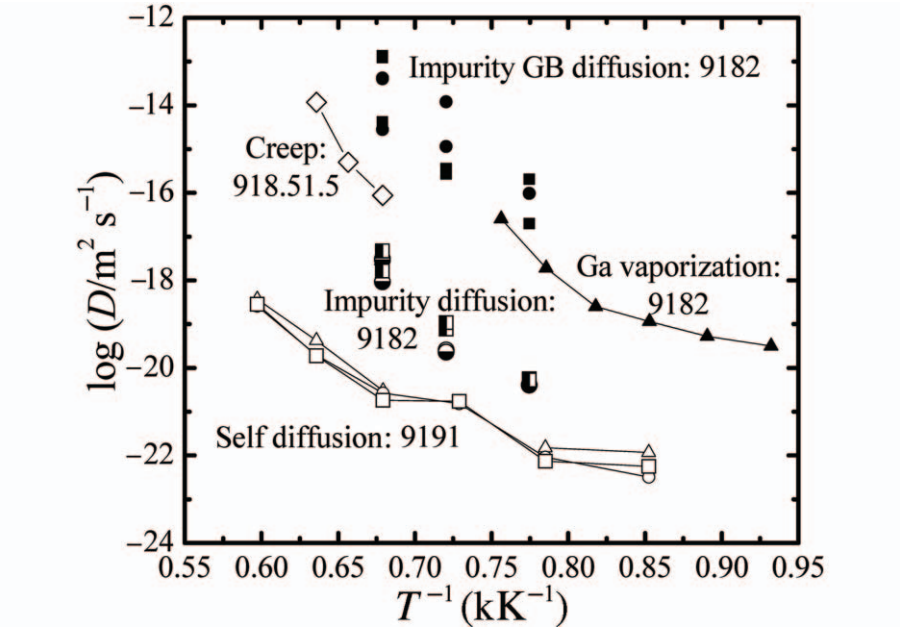

Figure 6. Cation diffusion D as a function of inverse temperature for (La,Se)(Ga,Mg)O_3 electrolytes: 9191 = $La_{0.9}Sr_{0.1}Ga_{0.9}Mg_{0.1}O_{2.9}$; 9182 = $La_{0.9}Sr_{0.1}Ga_{0.8}Mg_{0.2}O_{2.85}$; 918.51.5 = $La_{0.9}Sr_{0.1}Ga_{0.85}Mg_{0.15}O_{2.875}$. Data sources: creep data, Reference 31; impurity diffusion (squares, Co; circles, Fe; solid symbols for grain-boundary diffusion, half-solid symbols for bulk diffusion), Reference 2; self-diffusion (open squares, La; open circles, Sr; open triangles, Mg), Reference 32; vaporization, Reference 33.

with that of YSZ. This discrepancy can be explained in terms of fast grain-boundary diffusion, which is derived from diffusion couples with cathode materials.[2] High grain-boundary diffusion is also suggested from Ga vaporization experiments.[33]

For Further Development

In recent years, the R&D front for solid-oxide fuel cells has been widened to include lowering the operation temperature down to 500–600°C. To realize such SOFCs, one strategy is to use a thinner electrolyte, as suggested in Figure 2, where the temperature window is shown to be lower when the thickness of the electrolyte is reduced. However, the diffusion data presented here are quite suggestive that even at low temperatures, grain-boundary diffusion may affect the cell performance when thinner electrolytes are adopted. Furthermore, the driving force for chemical reactions is drastically changed with decreasing temperature.[34] It is for these reasons that a deeper understanding is required of equilibrium and transport properties in these materials.

References

1. H. Yokokawa and N. Sakai, in *Handbook of Fuel Cells,* Chapter 13, edited by W. Vielsich, A. Lamm, and H.A. Gasteiger (John Wiley & Sons, Chichester, U.K., 2003).
2. H. Yokokawa, N. Sakai, T. Horita, K. Yamaji, and M.E. Brito, *Electrochemistry* **73** (2005) p. 20.
3. N.S. Chadhury and J.W. Patterson, *J. Electrochem. Soc.* **118** (1971) p. 1398.
4. T. Kawada and H. Yokokawa, in *Electrical Properties of Ionic Solids,* edited by J. Nowotny and C.C. Sorrell (Trans Tech Publications, Zurich, 1997) p. 187.
5. H. Yokokawa, *Fuel Cells—From Fundamentals to Systems* **1** (2) (2001) p. 1.
6. Y.P. Xiong, K. Yamaji, T. Horita, N. Sakai, and H. Yokokawa, *J. Electrochem. Soc.* **151** (2004) p. A407.
7. T. Ishihara, M. Matsuda, and Y. Takita, *J. Am. Chem. Soc.* **116** (1994) p. 3801.
8. K. Yamaji, T. Horita, M. Ishikawa, N. Sakai, H. Yokokawa, and M. Dokiya, in *Solid Oxide Fuel Cells V,* PV97–40 (The Electrochemical Society, Pennington, N.J., 1997) p. 1041.
9. J.H. Kim and H.I. Yoo, *Solid State Ionics* **140** (2001) p. 105.
10. H. Yokokawa, in *Zirconia Engineering Ceramics: Old Challenges—New Ideas,* edited by Erich Kisi (Trans Tech Publications, Zurich, 1998) p. 37.
11. L. Minervini, M.O. Zacate, and R.W. Grimes, *Solid State Ionics* **116** (2000) p. 339.
12. M.O. Zacate, L. Ninervini, D.J. Bradfield, and R.W. Grimes, *Solid State Ionics* **128** (2000) p. 243.
13. J.A. Kilner, *Solid State Ionics* **129** (2000) p. 13.
14. M. Mogensen, N.M. Sammes, and G.A. Tompsett, *Solid State Ionics* **129** (2000) p. 63.
15. H. Yokokawa, T. Horita, N. Sakai, K. Yamaji, M.E. Brito, Y.-P. Xiong, and H. Kishimoto, *Solid State Ionics* **174** (2004) p. 205.

16. H. Yokokawa, *Annu. Rev. Mater. Res.* **33** (2003) p. 581.
17. H. Yokokawa, *J. Phase Equilib.* **20** (1999) p. 258.
18. H. Yokokawa, N. Sakai, T. Kawada, and M. Dokiya, *J. Electrochem. Soc.* **138** (1991) p. 2719.
19. T. Horita, K. Yamaji, M. Ishikawa, N. Sakai, H. Yokokawa, T. Kawada, and T. Kato, *J. Electrochem. Soc.* **145** (9) (1998) p. 3196.
20. D.M. Tricker and W.M. Stobbs, in *High Temperature Electrochemical Behavior of Fast Ion and Mixed Conductors,* edited by F.W. Poulsen, N. Bonamos, S. Linderoth, M. Mogensen, and B. Zachau-Christiansen (Risø National Laboratory, Roskilde, Denmark, 1993) p. 664.
21. H. Cerva, *J. Solid State Chem.* **120** (1995) p. 175.
22. T. Horita, K. Yamaji, N. Sakai, H. Yokokawa, and T. Kawada, and T. Kato, *Solid State Ionics* **127** (2000) p. 55.
23. T.S. Zhang, J. Ma, L.B. Kong, S.H. Chan, P. Hing, and J.A. Kilner, *Solid State Ionics* **167** (2004) p. 203.
24. C. Kleinlogel and L.J. Gauckler, *Solid State Ionics* **135** (2000) p. 567.
25. N. Sakai, K. Yamaji, T. Horita, H. Yokokawa, Y. Hirata, S. Sameshima, Y. Nigara, and J. Mizusaki, *Solid State Ionics* **125** (1999) p. 325.
26. S. Taniguchi, M. Kadowaki, H. Kawamura, T. Yasuo, Y. Akiyama, Y. Miyake, and T. Saitoh, *J. Power Sources* **55** (1995) p. 73.
27. Y. Matsuzaki and I. Yasuda, *J. Electrochem. Soc.* **148** (2001) p. A126.
28. T. Horita, K. Yamaji, T. Kato, N. Sakai, and H. Yokokawa, *J. Power Sources* **131** (2004) p. 299.
29. K. Huang, M. Feng, J.B. Goodenough, and M. Schmerling, *J. Electrochem. Soc.* **143** (1996) p. 3630.
30. K. Huang, J.H. Wan, and J.B. Goodenough, *J. Electrochem. Soc.* **148** (2001) p. A788.
31. J. Wolfenstine, *Solid State Ionics* **126** (1999) p. 293.
32. M. Martin and O. Schulz, in *Solid State Ionics: The Science and Technology of Ions in Motion,* edited by B.V.R. Chowdari, H.-L. Yoo, G.M. Choi, and J.-H. Lee (World Scientific, Singapore, 2004) p. 787.
33. K. Yamaji, H. Negishi, T. Horita, N. Sakai, and H. Yokokawa, *Solid State Ionics* **135** (2000) p. 389.
34. H. Yokokawa, N. Sakai, T. Kawada, and M. Dokiya, *Solid State Ionics* **52** (1992) p. 43. □